

DISCOVERY OF WASP-85 A b: A HOT JUPITER IN A VISUAL BINARY SYSTEM [†]

D. J. A. BROWN^{1,2}, D. R. ANDERSON³, D. J. ARMSTRONG¹, F. BOUCHY^{4,5}, A. COLLIER CAMERON⁶, L. DELREZ⁷, A. P. DOYLE¹, M. GILLON⁷, L. HEBB⁸, G. HÉBRARD^{4,5}, C. HELLIER³, E. JEHIN⁷, M. LENDL^{7,9}, P. F. L. MAXTED³, J. MCCORMAC¹, M. NEVEU-VANMALLE^{9,10}, D. POLLACCO¹, D. QUELOZ^{10,9}, D. SEGRANSAN⁹, B. SMALLEY³, O. D. TURNER³, A. H. M. J. TRIAUD^{11,9}, AND S. UDRY⁹

Draft version December 7, 2024

ABSTRACT

We report the discovery of the transiting hot Jupiter exoplanet WASP-85 A b. Using a combined analysis of spectroscopic and photometric data, we determine that the planet orbits its host star every 2.66 days, and has a mass of $1.09 \pm 0.03 M_{\text{Jup}}$ and a radius of $1.44 \pm 0.02 R_{\text{Jup}}$. The host star is of G5 spectral type, with magnitude $V = 11.2$, and lies 125 ± 80 pc distant. We find stellar parameters of $T_{\text{eff}} = 5685 \pm 65$ K, super-solar metallicity ($[\text{Fe}/\text{H}] = 0.08 \pm 0.10$), $M_{\star} = 1.04 \pm 0.07 M_{\odot}$ and $R_{\star} = 0.96 \pm 0.13 R_{\odot}$.

The system has a K-dwarf binary companion, WASP-85 B, at a separation of $\approx 1.5''$. The close proximity of this companion leads to contamination of our photometry, decreasing the apparent transit depth that we account for during our analysis. Without this correction, we find the depth to be 50 percent smaller, the stellar density to be 32 percent smaller, and the planet radius to be 18 percent smaller than the true value. Many of our radial velocity observations are also contaminated; these are disregarded when analysing the system in favour of the uncontaminated HARPS observations, as they have reduced semi-amplitudes that lead to underestimated planetary masses. We find a long-term trend in the binary position angle, indicating a misalignment between the binary and orbital planes. WASP observations of the system show variability with a period of 14.64 days, indicative of rotational modulation caused by stellar activity. Analysis of the Ca II H+K lines shows strong emission that implies that both binary components are strongly active. We find that the system is likely to be less than a few Gyr old.

WASP-85 lies in the field of view of K2 Campaign 1. Long cadence observations of the planet clearly show the planetary transits, along with the signature of stellar variability. Analysis of the K2 data, both long and short cadence, is ongoing.

Keywords: planets and satellites: detection – planets and satellites: individual: WASP-85 – techniques: photometric – techniques: radial velocities

d.j.a.brown@warwick.ac.uk

[†] based on observations (under proposal 089.C-0151(A)) made using the HARPS high resolution échelle spectrograph mounted on the ESO 3.6-m at the ESO La Silla observatory, and the IO:O camera on the 2.0-m Liverpool Telescope under program PL12B13.

¹ Department of Physics, University of Warwick, Coventry CV4 7AL

² Astrophysics Research Centre, School of Mathematics & Physics, Queen's University, University Road, Belfast, BT7 1NN, UK.

³ Astrophysics Group, School of Physical & Geographical Sciences, Lennard-Jones Building, Keele University, Staffordshire, ST5 5BG, UK.

⁴ Institut d'Astrophysique de Paris, UMR7095 CNRS, Université Pierre & Marie Curie, 98bis boulevard Arago, 75014 Paris, France

⁵ Observatoire de Haute Provence, CNRS/OAMP, 04870 St Michel l'Observatoire, France.

⁶ SUPA, School of Physics and Astronomy, University of St Andrews, North Haugh, St Andrews, Fife KY16 9SS, UK.

⁷ Institut d'Astrophysique et de Géophysique, Université de Liège, Allée du 6 Août, 17 (Bât. B5C) Sart Tilman, 4000 Liège, Belgium

⁸ Department of Physics and Astronomy, Vanderbilt University, Nashville, TN 37235, USA

⁹ Observatoire Astronomique de l'Université de Genève, Chemin des Maillettes 51, 1290 Sauverny, Switzerland

¹⁰ Cavendish Laboratory, J J Thomson Avenue, Cambridge, CB3 0HE, UK

¹¹ Kavli Institute for Astrophysics & Space Research, Massachusetts Institute of Technology, Cambridge, MA 02139, USA

1. INTRODUCTION

The study of extra-solar planets has been driven forward by the discovery and detailed analysis of those planets that transit the disc of their host star. These transiting systems provide information on the planet’s radius (e.g. Charbonneau et al. 2000) and absolute mass, information that is vital for the accurate characterisation of both the planet and star. Planets transiting bright stars ($8.5 < V < 12.5$) are particularly prized; they enable detailed follow-up studies that can provide confirmation of the planets’ existence, as well as allowing the exploration of the planets’ characteristics, such as spin-orbit alignment and atmospheric composition.

The space-based Kepler (Borucki et al. 2010) transit survey mission has vastly expanded the size of the exoplanet population, and has discovered small, Earth-like planets, circumbinary planets, and multi-planet systems that are inaccessible to instruments on the ground. It is the ground-based surveys though, such as the Wide Angle Search for Planets (WASP; Pollacco et al. 2006), HATnet (Bakos et al. 2002), TrES (Alonso et al. 2004), XO Project (McCullough et al. 2005), and KELT (Pepper et al. 2007), that are leading the way in the discovery of planets orbiting bright stars. WASP is by far the most successful of these surveys, with more than 100 published planet discoveries to date.

A recent study of F, G, and K stars in the Sloan Digital Sky Survey (SDSS) showed that approximately 43 ± 2 percent of solar-type stars have binary companions with periods of < 1000 days (Gao et al. 2014). This supports earlier results by Raghavan et al. (2010) (46 ± 2 percent solar type stars in binaries), Duquennoy & Mayor (1991), and Abt & Levy (1976), among others. However, the binary fraction seems to be lower for exoplanet systems (Roell et al. 2012), indicating a suppression of planet formation (Wang et al. 2014). There is a strong selection effect acting against binary systems in planet search programs, that Roell et al. acknowledge and Wang et al. correct for. The presence of a companion star to the planet host introduces the problem of light from said star contaminating either the photometric observations (diluting the transit depth), spectroscopic observations (introducing a second set of spectral lines, and thus a second cross-correlation function peak), or both. The level of contamination depends on several factors - the resolution of the instrument, aperture size, fibre diameter, seeing, the separation of the stars, and the magnitude difference between the stellar components. These factors vary considerably from system to system, and the presence of a binary companion to an exoplanet candidate star tends to reduce the likelihood of that candidate becoming the target of follow-up observations.

Nevertheless, there are several examples of hot Jupiter exoplanets in S-type orbits around binary stars, including WASP-70 A b (Anderson et al. 2014); WASP-77 A b (Maxted et al. 2013); WASP-94 A b and B b (Neveu-VanMalle et al. 2014); Kelt-2 A b (Beatty et al. 2012), and Kepler-14 A b (Buchhave et al. 2011). Analysis of the known planets in binary systems deal with the contamination in different ways. For their analysis of WASP-70 A b, Anderson et al. (2014) corrected the photometric data using flux ratios derived from

their observations. A similar approach was taken by Neveu-VanMalle et al. (2014) for WASP-94 A b, and by Maxted et al. (2013) for WASP-77 A. Kepler-14 A b is possibly the most similar system to that we consider here, and Buchhave et al. (2011) account for the dilution by placing a prior on the flux ratio of the binary components. The most complex approach is that of Beatty et al. (2012) for Kelt-2 A b, who carry out an iterative combination of Markov Chain Monte Carlo analysis and SED fitting to constrain the transit depth.

In this paper we present the discovery of WASP-85 A b, a transiting hot Jupiter exoplanet with mass $M_p = 1.09 \pm 0.03 M_{\text{Jup}}$ and radius $R_p = 1.44 \pm 0.02 R_{\text{Jup}}$. The solar-type host star, WASP-85 A is the brighter component of a close visual binary, BD+07°2474, while the companion star, WASP-85 B, is cooler than the host star, but of similar magnitude. The presence of the companion star complicates the standard analysis procedure used for WASP planets; we account for the 3rd light contamination by adding an additional term to our stellar model, derived from our photometric data and controlled by a Markov Chain Monte Carlo jump parameter and prior. There is a clear, long-term trend in the position angle between the binary components, which indicate an orbit of ≈ 3000 years for the binary. The system lies in the field of view of K2 Campaign 1, and was observed in both long and short cadence modes. The K2 light curve clearly shows the planetary transits, along with the signature of stellar variability. Analysis of the K2 data from both observing modes is ongoing, and will be presented in a follow-up paper.

In Section 2 we detail the photometric and spectroscopic observations of the WASP-85 system, while in Section 3 we discuss the methods by which we derive the system parameters. We discuss the characteristics of the star and planet in Section 4, and conclude by summarising our results in Section 5. Throughout the manuscript we use the TDB time standard and Barycentric Julian Dates in our analysis, following the advice set out in Eastman, Siverd, & Gaudi (2010). Our results are based on the equatorial solar and jovian radii, and masses taken from Allen’s Astrophysical Quantities.

2. OBSERVATIONS

2.1. WASP photometry

For a detailed account of the WASP telescopes, observing strategy, data reduction, and candidate identification and selection procedures, see Pollacco et al. (2006, 2008) and Collier Cameron et al. (2007).

BD+07°2474 lies near the celestial equator, and was thus observed by both SuperWASP-North (located at the Observatorio del Roque de los Muchachos on La Palma, Spain) and WASP-South (located at the South African Astronomical Observatory near Sutherland, South Africa). These observations resulted in 20936 data, spanning the period 2008-02-05 to 2011-03-29.

The system was first identified as a planet candidate from SuperWASP-North data in 2008. Initial analysis revealed transit like features with an apparent period of ≈ 1.59 days. This signal was subsequently identified in both the SuperWASP-North and WASP-South photometry independently, and the star was selected for photo-

metric and spectroscopic follow-up observations. Subsequent to these observations, the secondary peak in the periodogram, at ≈ 2.66 days, was found to be the correct period.

The radius of the synthetic aperture ($48''$) used to extract the flux of BD+07°2474 is much greater than the maximum binary separation ($1.8''$); see Section 4.2), such that the WASP lightcurve includes flux contributions from both components of the binary.

2.2. Spectroscopic follow-up

Initial spectroscopic reconnaissance was carried out between 2008 and 2010 using the SOPHIE spectrograph (Perruchot et al. 2008; Bouchy et al. 2009) mounted on the 1.93-m telescope of the Observatoire de Haute-Provence (OHP), resulting in the acquisition of 11 spectra. RVs were derived through cross-correlation with a spectral mask suitable for a star of G2 spectral type. The separation of the binary components is smaller than the fibre diameter of SOPHIE ($3''$), and thus the radial velocities (RVs) obtained from this instrument are contaminated by the contribution of the companion. These data show a sinusoidal variation in radial velocity (RV) with a period of ≈ 2.66 days, in disagreement with the period identified in the WASP lightcurves.

Further spectroscopic observations were made using the fibre-fed CORALIE spectrograph at the Euler-Swiss telescope at ESO’s La Silla observatory, and using HARPS at the ESO 3.6m telescope, also at La Silla. A total of 31 observations were made using CORALIE between 2009 January 03 and 2014 June 24. For details of the instrument and data reduction procedure, see Queloz et al. (2000) and Wilson et al. (2008). RVs were derived using cross-correlation with a spectral mask suitable for a G2-type star, and confirmed the ≈ 2.66 day period as the correct one. Unfortunately, while the CORALIE guiding camera is able to identify the presence of both stellar components, the aperture of the spectrograph ($2''$) is insufficiently small to access a single stellar component at a time. The CORALIE spectra are therefore also contaminated by light from the companion star. The level of contamination is seeing dependent owing to the close similarity of the aperture size and binary separation, rendering a correction to the RVs both uncertain and difficult to make.

Eight observations of the brighter binary component (hereafter WASP-85 A), and five observations of the fainter companion star (hereafter WASP-85 B) were made using HARPS. The small spectrograph aperture ($1''$ diameter) and good seeing allowed the components to be observed separately, with little contamination from the other star. RVs were extracted in the same manner as for the CORALIE observations.

We check for false positives induced by background eclipsing binaries or stellar activity by examining the bisector span measurements for our data. We find no significant correlation with the radial velocities or the radial velocity residuals, although the observations for WASP-85 B do seem to show a negative correlation between the parameters. This is indicative of stellar activity (Queloz et al. 2001). We also plot the full widths at half maximum (FWHM) of our radial velocity observations as a function of orbital phase, checking for variations in phase (Santerne, Moutou, & Bouchy 2011).

None are seen (see Figure 1). We confirm which binary component is the planet host by checking for phasing of the HARPS radial velocity observations. The observations of WASP-85 A show variations in phase with both the photometry, and with the CORALIE and SOPHIE observations, while the observations of WASP-85 B show variations that are not correlated with the phase determined from the lightcurve.

We list our RV data in Table 1, along with the bisector spans, which measure the asymmetry of the cross-correlation functions (CCFs), and the FWHMs of the CCFs. Uncertainties on the bisectors were taken to be twice the uncertainty on the RV, while those on the FWHMs were taken to be 2.35 times the RV uncertainty.

2.3. Photometric follow-up

Follow-up photometric observations to solidify the planet’s ephemeris, and check for transit timing shifts, were carried out using the James Gregory Telescope (JGT) at the University of St Andrews Observatory, the robotic Transiting Planets and Planetesimals Small Telescope (TRAPPIST; Jehin et al. 2011) at La Silla, the Euler-Swiss telescope using EulerCam (Lendl et al. 2012), also at La Silla, and the Liverpool Telescope (LT; Steele et al. 2004) on La Palma using the IO:O instrument. These observations are summarised in Table 2.

The resolutions and pixel scales of the telescopes and instruments used for photometric follow-up were insufficient to distinguish the companion star. All lightcurves are therefore of the blended combination of light from the two stellar components.

3. ANALYSIS

3.1. Stellar parameters

We co-added all of the individual HARPS spectra of WASP-85 A and WASP-85 B to produce a single spectrum with a typical S/N of around 60:1 and 30:1, respectively. The standard pipeline reduction products were used in the analysis, which was performed using the methods given in Doyle et al. (2013). The effective temperature (T_{eff}) was determined from the excitation balance of the Fe I lines. The Na I D lines, the Ca I line at 6439 \AA , and the ionisation balance of Fe I and Fe II were used as surface gravity ($\log g_*$) diagnostics. The metallicity was determined from equivalent width measurements of several unblended lines. A value for microturbulence (ξ_t) was determined from Fe I using the method of Magain (1984).

The projected stellar rotation velocity ($v \sin I_*$) was determined by fitting the profiles of several unblended lines. Values for macroturbulence (v_{mac}) of 2.93 ± 0.73 and $2.20 \pm 0.73 \text{ km s}^{-1}$ were determined from the calibration of Doyle et al. (2014). A best fit value of $v \sin I_* = 3.41 \pm 0.89$ and $3.32 \pm 0.82 \text{ km s}^{-1}$ were obtained for WASP-85 A and WASP-85 B, respectively.

The results are summarised in Table 3; the quoted uncertainties account for the errors in T_{eff} and $\log g_*$ as well as the additional scatter induced by measurement and atomic data uncertainties. The spectral type was estimated from T_{eff} using Table B.1 in Gray (2008), while the stellar mass and radius estimates were derived using the Torres et al. (2010) calibration.

Table 1
Radial velocity data of WASP-85 A and WASP-85 B, obtained using HARPS, and of the two components combined, obtained using SOPHIE and CORALIE.

BJD _{TDB} −2450000 (days)	RV (km s ^{−1})	σ _{RV} (km s ^{−1})	Bisector (km s ^{−1})	σ _{bis} (km s ^{−1})	FWHM (km s ^{−1})	σ _{FWHM} (km s ^{−1})
<i>SOPHIE</i>						
4820.64118	13.579	0.024	−0.012	0.048	10.100	0.056
4821.64438	13.367	0.019	0.004	0.0038	10.059	0.045
4822.60638	13.506	0.017	−0.010	0.034	9.976	0.040
4823.61708	13.565	0.016	−0.017	0.032	9.949	0.038
4824.70288	13.365	0.015	0.017	0.030	9.855	0.035
4824.72498	13.363	0.015	0.001	0.030	9.851	0.035
4834.64438	13.417	0.017	−0.006	0.034	10.023	0.040
4835.64718	13.389	0.016	0.007	0.032	9.964	0.038
4836.60168	13.586	0.017	−0.003	0.034	9.956	0.040
5304.44298	13.533	0.013	−0.006	0.026	9.924	0.031
5305.39608	13.386	0.013	−0.011	0.026	9.974	0.031
<i>CORALIE</i>						
4834.834967	13.42322	0.00643	−0.00053	0.01286	8.91982	0.01511
4836.811531	13.58281	0.00719	−0.03262	0.01438	8.93960	0.01690
5675.670857	13.67921	0.00577	0.01552	0.01154	8.87000	0.01356
5676.638783	13.42716	0.00652	0.00368	0.01304	8.85258	0.01532
5677.666565	13.53687	0.00696	0.00109	0.01382	8.89084	0.01636
5679.634306	13.42072	0.00577	−0.01245	0.01154	8.82570	0.01356
5684.661489	13.42964	0.00617	−0.03682	0.01234	8.85497	0.01450
5706.548896	13.45416	0.00613	0.00763	0.01226	8.83622	0.01441
5707.572297	13.67309	0.00644	0.00705	0.01288	8.84507	0.01513
5712.520574	13.53203	0.00614	−0.00174	0.01228	8.85190	0.01443
5715.509353	13.67937	0.00582	−0.03608	0.01164	8.84725	0.01368
6020.746523	13.69205	0.00663	−0.01937	0.01326	8.89409	0.01558
6030.562877	13.41197	0.01331	0.00647	0.02662	8.87074	0.03128
6031.594135	13.65143	0.00757	−0.02514	0.01514	8.86701	0.01779
6031.738294	13.64104	0.01067	−0.01863	0.02134	8.85919	0.02507
6032.538879	13.37756	0.00838	−0.02683	0.01676	8.85724	0.01969
6067.600608	13.44722	0.00618	0.00095	0.01236	8.79800	0.01452
6068.533616	13.66361	0.00625	−0.04270	0.01250	8.81772	0.01469
6069.488518	13.46423	0.00933	−0.00556	0.01866	8.84598	0.02193
6070.519073	13.49368	0.00767	−0.00073	0.01534	8.82180	0.01802
6071.591742	13.65052	0.00686	−0.02006	0.01372	8.81989	0.01612
6116.471681	13.69886	0.00569	0.00593	0.01138	8.79002	0.01337
6339.779756	13.66741	0.00689	−0.00840	0.01378	8.89293	0.01619
6341.810736	13.61604	0.00753	−0.04102	0.01506	8.89167	0.01770
6342.674625	13.57377	0.00815	−0.02626	0.01630	8.93949	0.01915
6362.859062	13.54098	0.01032	0.00550	0.02064	8.87031	0.02425
6365.798530	13.63578	0.00726	−0.01186	0.01452	8.89014	0.01706
6366.844086	13.51656	0.00874	−0.00777	0.01748	8.87421	0.02054
6697.826971	13.64283	0.00695	−0.03800	0.01390	8.98653	0.01633
6741.736317	13.43313	0.00603	−0.02803	0.01206	8.88454	0.01417
6833.496459	13.67453	0.00717	−0.03279	0.01434	8.86483	0.01685
<i>HARPS star A</i>						
6020.588912	13.74735	0.00316	−0.00958	0.00632	7.59818	0.00743
6020.736685	13.76810	0.00337	0.00149	0.00674	7.61603	0.00792
6028.594310	13.73631	0.00405	−0.01231	0.00810	7.58601	0.00952
6029.582170	13.55755	0.00467	−0.02840	0.00934	7.61188	0.01097
6029.742186	13.50857	0.00598	0.00692	0.01196	7.59248	0.01405
6030.572124	13.45497	0.01833	−0.05632	0.03666	7.54788	0.04308
6031.573927	13.72069	0.00478	−0.01092	0.00956	7.60938	0.01123
6032.541680	13.46784	0.00449	−0.01581	0.00898	7.60061	0.01055
<i>HARPS star B</i>						
6020.602442	13.07700	0.00573	−0.01224	0.01146	7.90081	0.01347
6020.745898	13.09952	0.00558	−0.02263	0.01106	7.88332	0.01311
6028.603233	13.15039	0.00614	−0.04569	0.01228	7.84657	0.01443
6029.591232	13.13818	0.00822	−0.02829	0.01644	7.84906	0.01932
6029.750461	13.18411	0.00863	−0.02544	0.01726	7.76341	0.02028

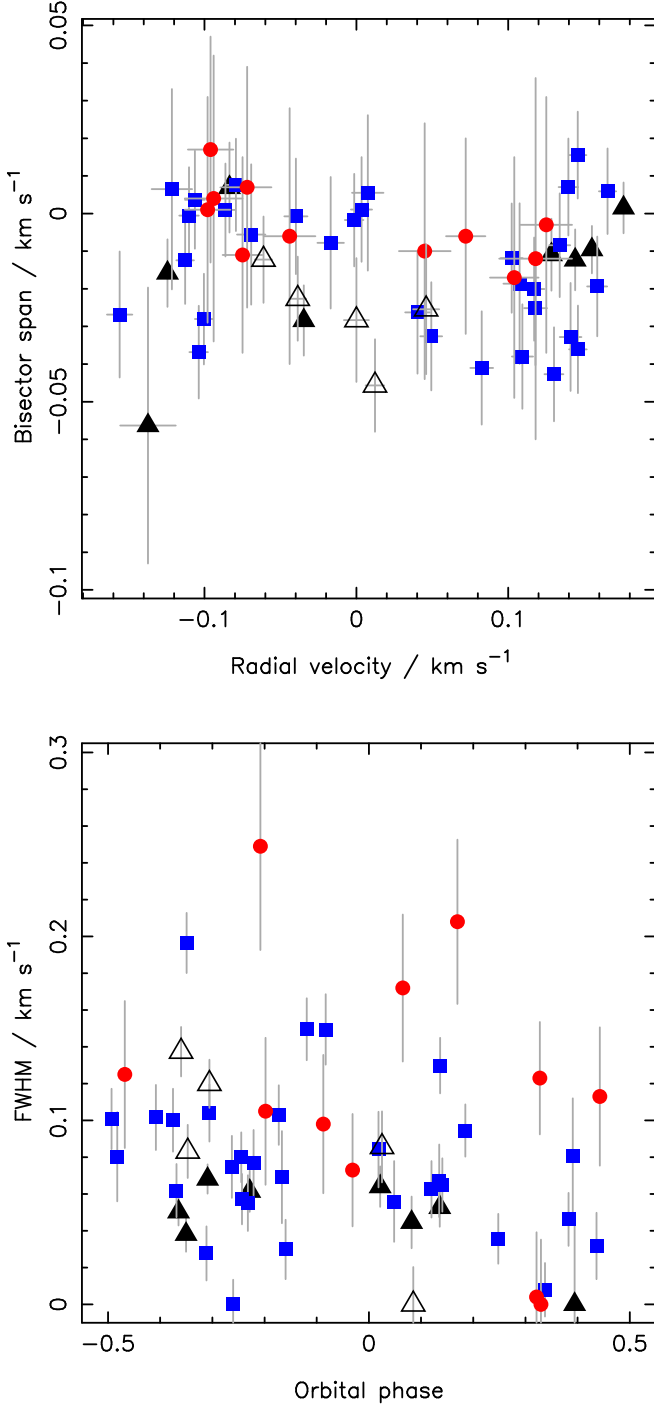


Figure 1. *Upper panel:* Radial velocity bisector span plotted as a function of relative radial velocity. The uncertainties in the bisector measurements are taken to be $2.0 \times \sigma_{RV}$. HARPS data for WASP-85 A are denoted by solid, black triangles, data for WASP-85 B by open, black triangles. CORALIE data are denoted by solid, blue squares. SOPHIE data are denoted by solid, red circles. Only the WASP-85 B data show a negative correlation between the two parameters. *Lower panel:* Radial velocity full width at half maximum (FWHM) as a function of orbital phase. The uncertainties in the FWHMs are taken to be $2.35 \times \sigma_{RV}$. The FWHM values have been offset from the minimum value for each data set to allow comparison. There is no clear variation with orbital phase.

Table 2
Summary of photometric follow-up observations.

Instrument	Date	Time of observations	Filter	N_{data}
JGT	2009-03-20	21 : 43 – 01 : 42	Cousins R	237
IO:O	2013-01-12	02 : 39 – 06 : 41	Sloan z'	146
IO:O	2013-01-28	01 : 18 – 05 : 15	Sloan z'	146
EulerCAM	2013-03-23	04 : 23 – 07 : 55	RG	186
TRAPPIST	2013-03-31	03 : 39 – 08 : 07	Sloan z'	569
TRAPPIST	2013-04-16	01 : 56 – 06 : 41	Sloan z'	615
TRAPPIST	2013-05-09	23 : 52 – 04 : 10	Sloan z'	503
TRAPPIST	2013-05-25	22 : 47 – 03 : 02	Sloan z'	626

Note: The RG filter used in EulerCAM is a modified broad Gunn-R filter, with a central wavelength of 660 nm. A slewing problem affected TRAPPIST during the transit on 2013-03-31, leading to gaps in coverage.

Table 3
Summary of the stellar parameters derived using spectroscopic analysis.

Parameter	WASP-85 A	WASP-85 B	Units
RA	11h43m38.01s		J2000
DEC	+06°33'49.4'		J2000
V	11.2	11.9	Tycho
$B-V$	0.670 ± 0.022	$0.828^{+0.034}_{-0.036}$	
Distance		125 ± 80	pc
Spectral type	G5	K0	
T_{eff}	5685 ± 65	5250 ± 90	K
Mass, M_{\star}	1.04 ± 0.07	0.88 ± 0.07	M_{\odot}
Radius, R_{\star}	0.96 ± 0.13	0.77 ± 0.13	R_{\odot}
$\log g_{\star}$	4.48 ± 0.11	4.61 ± 0.14	cgs
ξ_t	0.6 ± 0.1	0.9 ± 0.1	km s^{-1}
v_{mac}	2.93 ± 0.73	2.20 ± 0.73	km s^{-1}
$v \sin I_{\star}$	3.41 ± 0.89	3.32 ± 0.82	km s^{-1}
P_{rot}		14.6 ± 1.5	days
$\log A(\text{Li})$	2.19 ± 0.06	$< 0.70 \pm 0.10$	
[Fe/H]	0.08 ± 0.10	0.00 ± 0.15	
$\log(R'_{\text{hk}})$	$-4.43^{+0.06}_{-0.02}$	$-4.37^{+0.09}_{-0.04}$	

Note: Masses and radii estimated using the calibration of Torres et al. (2010). Spectral Type estimated from T_{eff} using Table B.1 in Gray (2008). Abundances are relative to the solar values obtained by Asplund et al. (2009). The rotation period is the mean of the periods determined from a periodogram analysis of the WASP lightcurve.

3.1.1. Stellar activity

Using the HARPS spectra with $S/N > 4$ for the core of the Ca II H+K lines, we calculate the $\log(R'_{\text{hk}})$ activity index using the emission in the cores of the Ca II H+K lines following Noyes et al. (1984). We find an activity index of $\log(R'_{\text{hk}}) = -4.43^{+0.06}_{-0.02}$ for WASP-85 A. For WASP-85 B we find $\log(R'_{\text{hk}}) = -4.37^{+0.09}_{-0.04}$ using spectra with $S/N > 2$.

We carried out a search for stellar modulation in the WASP lightcurve using the method described in Section 4 of Maxted et al. (2011). The WASP data were separated according to the year of observation, as starspot

Table 4

Results from the periodogram analysis of the four seasons of WASP data for the WASP-85 system.

Year	N_{data}	Period (days)	Amp	FAP
2008	2559	6.644	0.003	0.0389
2009	6760	15.600	0.003	0.0011
2010	8157	13.130	0.003	0.0000
2011	2442	16.550	0.003	0.0002
Adopted		14.6 ± 1.5		

induced variability is not expected to be coherent on long timescales owing to the short lifetime of magnetic features on the the stellar surface. The transit features were subtracted using the best fit model transit model for that year. A modified, generalised Lomb-Scargle periodogram (e.g. Zechmeister & Kürster 2009), computed using the method of Press & Rybicki (1989) over 4096 uniformly spaced frequencies from 0 to 2.5 cycles/day, was used to search for significant periodicity in the lightcurves. The resulting periodograms are shown in Figure 2, and the results for the most significant peak are given in Table 4. False alarm probabilities (FAP) were calculated using a Monte Carlo bootstrap method (Maxted et al. 2011).

In the 2009, 2010, and 2011 data there are significant peaks at approximately 15 days. We associate this with the stellar rotation of one of the stellar components. The shorter period found in the 2008 data is approximately $P_{\text{rot}}/2$, and easily explained by the presence of two active regions on opposite sides of the star. This would produce a photometric signature at twice the rotational frequency, and will contribute power in other seasons as well, but less dominantly. Note that there is significant power at periods close to 1 day in all four seasons. This likely arises as a result of the diurnal observing schedule forced upon WASP by its ground-based nature.

We estimate a mean rotation period of 14.6 ± 1.5 days using the results from all four seasons. This value is in good agreement with the rotation period of 14.2 ± 4 d implied by the values of $v \sin I_*$ and the stellar radius of WASP-85 A. However it is also in agreement with the rotation period of 11.7 ± 4 days implied for WASP-85 B, making it impossible to determine which star the rotational modulation originates from using this data alone. We will discuss this result further in Section 4.

We whiten the four sets of data by fitting a harmonic series with $P_0 = P_{\text{rot}}/2$ as the fundamental period. The number of terms in the series was determined by minimising the Bayesian Information Criterion (Schwarz 1978). The resulting fit was divided-out, and the lightcurves concatenated to produce a whitened WASP lightcurve.

3.1.2. Stellar age

Lithium is detected in WASP-85 A, with an equivalent width of 53 mÅ, corresponding to an abundance of $\log A(\text{Li}) = 2.19 \pm 0.06$. This implies an age of between 0.5 and 2.0 Gyr. There is no significant detection of lithium in WASP-85 B, with an equivalent width up-

Table 5

Age constraints for the two binary components, as determined using a variety of techniques.

Method	Ages WASP-85 A (Gyr)	WASP-85 B (Gyr)
<i>Lithium abundance</i>		
log A(Li)	0.5 – 2.0	> 0.6
<i>Isochrone placement</i>		
Padova	$0.68^{+0.88}_{-0.64}$	> 0.08
YY	1.33 – 2.57	–
DSED	$2.42^{+2.27}_{-1.91}$	–
GARSTEC	2.2 ± 1.6	–
<i>Gyrochronology</i>		
P_{rot}	$1.53^{+0.32}_{-0.28}$	
$v \sin I_*$	$< 1.45^{+1.25}_{-0.58}$	$< 0.81^{+0.61}_{-0.30}$
<i>Activity</i>		
MamaJek	$0.37^{+0.09}_{-0.15}$	$0.26^{+0.12}_{-0.16}$

per limit of 2 mÅ, corresponding to an abundance upper limit of $\log A(\text{Li}) < 0.70 \pm 0.10$, and implying an age of several Myr (Sestito & Randlich 2005).

Stronger age constraints can be evaluated through a comparison to theoretical stellar models. We use the isochrone placement method of Brown (2014), working in the $[\rho_*^{-1/3}, T_{\text{eff}}]$ parameter space suggested by Sozzetti et al. (2007). We evaluate the age of each component using three sets of stellar models: the Padova models of Marigo et al. (2008); Girardi et al. (2010); the Yonsei-Yale (YY) isochrones of Demarque et al. (2004), and models from the Dartmouth Stellar Evolution Database (DSED; Dotter et al. 2008). We used independent measurements of T_{eff} (derived from the stellar spectra) and ρ_* (derived directly from the photometric lightcurves during the transit modelling process, see Section 3.2) to derive the stellar ages at the central value of $[\text{Fe}/\text{H}]$ listed in Table 3, and at its 1σ limits. The results are listed in Table 5.

We also carry out a Bayesian isochrone fitting process in $[\log(L_*), T_{\text{eff}}]$ parameter space, using the GARSTEC models of Weiss & Schlattl (2008), as computed by Serenelli et al. (2013). This new method is detailed in Maxted, Serenelli & Southworth (2014). Using this method we find an age of 2.2 ± 1.6 Gyr for WASP-85 A using $[\text{Fe}/\text{H}] = 0.10$.

In addition, we estimate the age of the two components using their measured and estimated rotation periods. We use the gyrochronology formulation of Barnes (2010), calculating the convective turnover timescale using Table 1 of Barnes & Kim (2010) and setting $P_0 = 1.1$ d. Using the measured rotation period, we derive a gyrochronological age of $1.53^{+0.32}_{-0.28}$ Gyr. It is also possible to derive gyrochronological ages using the projected rotation velocity to derive an upper limit on the rotation period. Ages derived in this manner will also therefore be upper limits. The rotation rate ($P_{\text{rot}} = 14.2 \pm 4$ d) implied

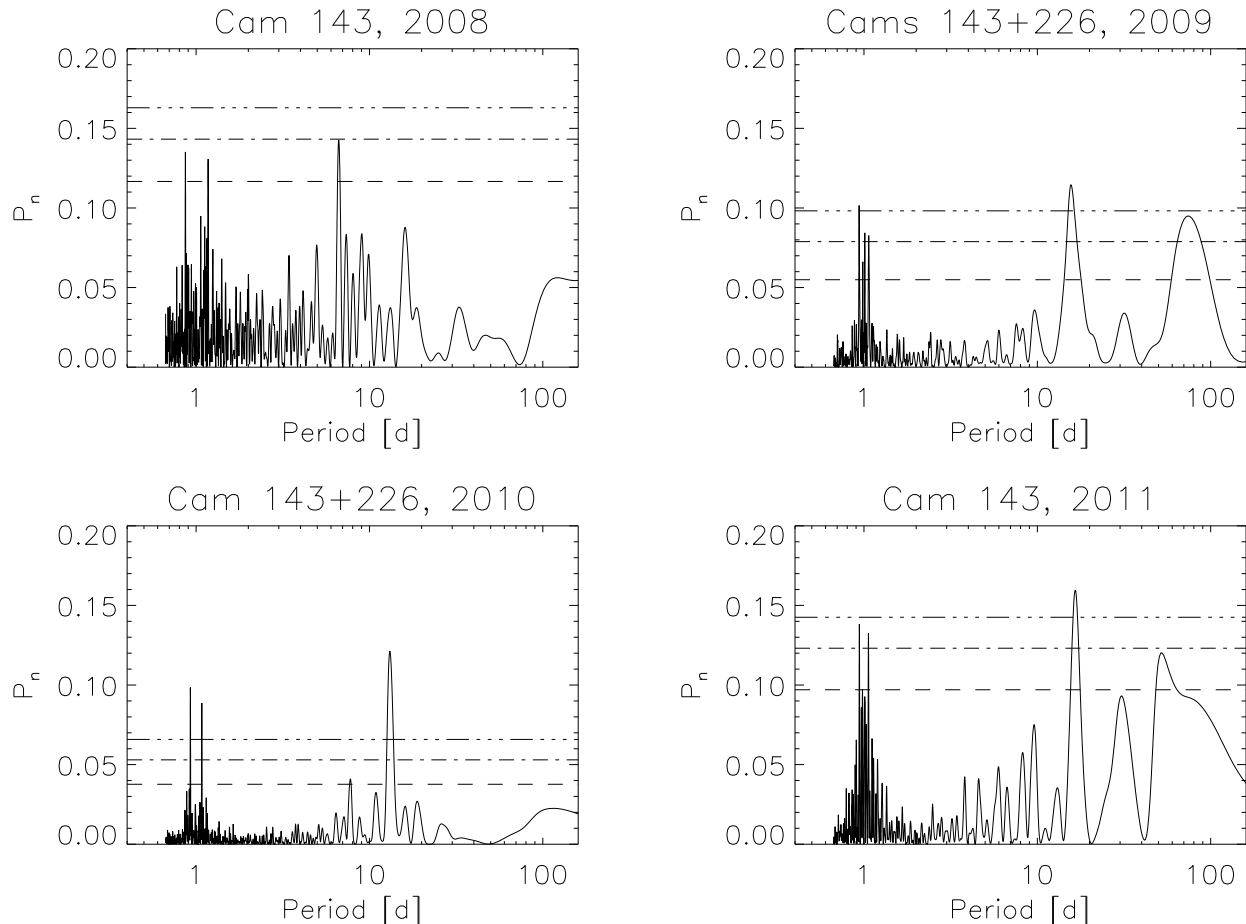


Figure 2. Periodograms for the four seasons of WASP data for the WASP-85 system. The year is given in the title of each panel. The horizontal lines indicate false-alarm probability levels of $FAP = 0.1, 0.01, \text{ and } 0.001$. Note the changing scale of the y-axis. In 2009, 2010, and 2011, a significant peak is seen at approximately 15 days. We associate this with the rotation period of one of the stars, though it is impossible to determine which star given the data available. The strongest peak in the 2008 data is at approximately half of this period.

by the measured $v \sin I_*$ for WASP-85 A gives an age of $< 1.45^{+1.25}_{-0.58}$ Gyr, in good agreement with this. The implied rotation rate ($P_{\text{rot}} = 11.7 \pm 4$ d) for WASP-85 B gives an age of $< 0.81^{+0.61}_{-0.30}$ Gyr, which would seem to imply that the detected rotation period is that of WASP-85 A. However, given the contamination of the WASP photometry we cannot be certain.

Finally, we estimate the age for the two components using the stellar activity - age relation of Mamajek & Hillenbrand (2008). We find ages of $0.37^{+0.06}_{-0.14}$ Gyr and $0.24^{+0.09}_{-0.13}$ Gyr for stellar components A and B, respectively.

The ages for WASP-85 A that we derive using the four different isochrone analyses are consistent, and are also in agreement with the gyrochronology ages that we derive from the detected rotation period, and from $v \sin I_*$. The age that we determine using the chromospheric activity index is younger than many of the other estimates, but does agree with the Padova isochrone age.

If we assume that the stars are gravitationally bound, as seems likely given the similar radial velocities that we measure for the two stars, and the fact that we see only a single CCF in the CORALIE and SOPHIE spectrum,

then it is encouraging that the results for the two stars agree. We note though that the constraints on WASP-85 B's age are very loose.

3.2. Planetary and orbital parameters

To determine the planetary and orbital parameters, we carry out a simultaneous analysis of the HARPS RVs for WASP-85 A, and the full suite of photometric observations. This allows us to fully account for inter-parameter correlations, and properly characterise the uncertainties in the system parameters. We elect not to include the RV data obtained using CORALIE and SOPHIE owing to the aforementioned, unknown contamination caused by the presence of the companion star. It is possible to correct the contaminated RVs through careful analysis of the CCFs, given that we have data for the two components separately from HARPS observations. Buchhave et al. (2011) describe another means by which contaminated CCFs can be corrected that applies shifts to the spectrum and co-adds the results to the observed spectrum divided by a constant determined by the flux ratio. Given our access to uncontaminated HARPS data we elect not to perform a correction; we leave this as a problem for a more detailed follow-up analysis of the system in the

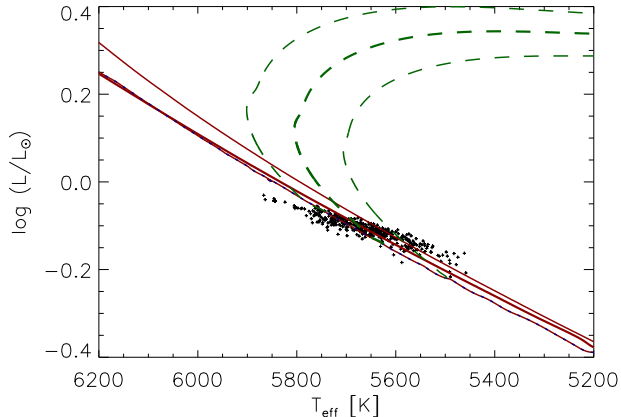


Figure 3. Hertzsprung-Russell diagram showing the results of a Bayesian analysis of WASP-85 A’s age. The red, solid lines represent isochrones of 0.0, 1.08, and 2.66 Gyr, while the green, dashed lines represent representative evolutionary models of 0.98, 1.02, and 1.06 M_{\odot} , all computed for $[Fe/H]_{\text{initial}} = 0.10$. Black dots mark individual steps in the Markov chain; we display only a random selection of 1000 data to improve clarity.

future.

We carry out our analysis using a modified version of the Markov Chain Monte Carlo (MCMC) code described in Collier Cameron et al. (2007), Pollacco et al. (2008), and Brown et al. (2012). To recap, this models the RVs with a Keplerian orbit, while the transits are fitted using the photometric model of Mandel & Agol (2002). We account for limb-darkening using a non-linear model with four components; we derive wavelength appropriate coefficients for each photometric dataset by interpolating through the tables of Claret (2000, 2004) at each MCMC step. We also carry out a linear decorrelation in phase at each step to remove systematic trends in the photometric data; owing to the presence of an additional trend in the LT / IO:O lightcurves (probably secondary extinction), we found it necessary to use a quadratic decorrelation in phase for the two lightcurves obtained with that instrument. We add an additional stellar “jitter” term of 7.5 m s^{-1} to the formal RV uncertainties in order to obtain a reduced spectroscopic $\chi^2 \approx 1$.

The following jump parameters are used as standard: the epoch of mid-transit, T_0 ; the orbital period, P ; the full transit duration, T_{dur} ; the planet:star area ratio, R_p^2/R_{\star}^2 ; the impact parameter for a circular orbit, b ; T_{eff} ; $[Fe/H]$, and the RV semi-amplitude, K . We apply priors on $v \sin I_{\star}$, T_{eff} and $[Fe/H]$ using the spectroscopic values listed in Table 3, in all cases assuming a Gaussian distribution. Steps are accepted using the Metropolis-Hastings algorithm, with a scale factor set to ensure an acceptance rate of roughly 25 percent.

For WASP-85, we add a number of additional jump parameters equal to the number of photometric datasets. These are the third light contributions to each transit, $L_{3,i}$, defined as the flux ratio of the two components F_B/F_A , and allow us to account for the dilution induced by the presence of the binary companion. We apply a Bayesian prior on each of the $L_{3,i}$, assuming a Gaussian distribution; for the observations in the Sloan z’ band we use the flux ratio of 0.54 ± 0.02 measured in the course

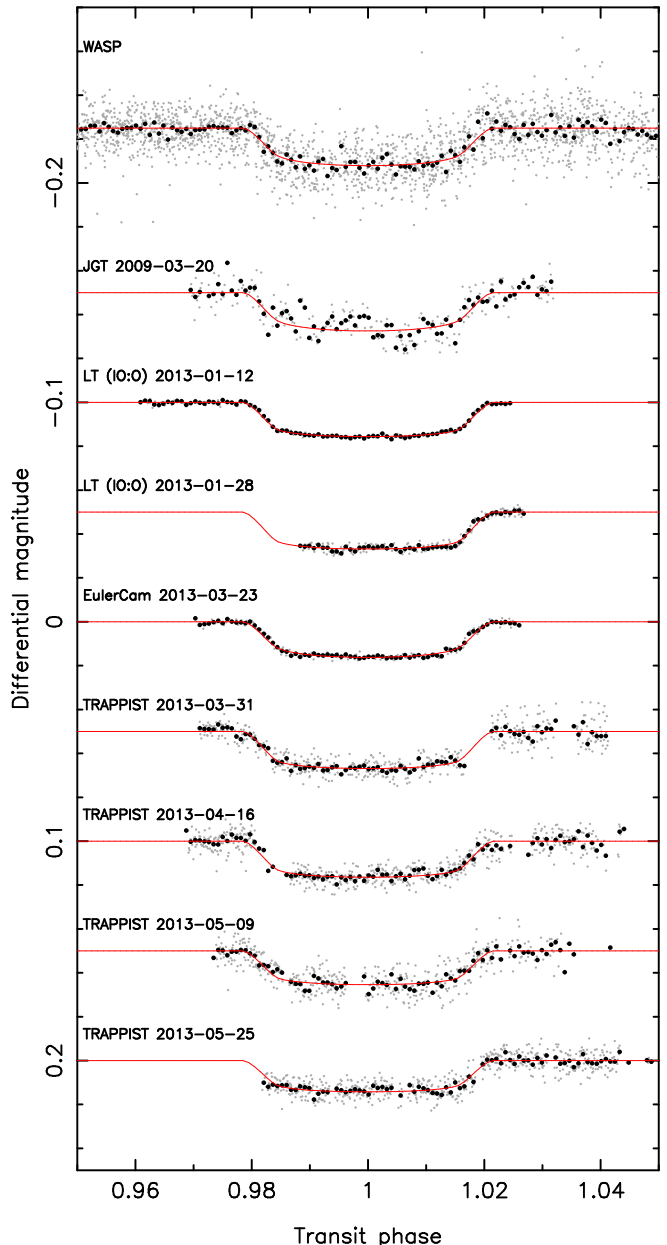


Figure 4. Photometric transit lightcurves of the WASP-85 system. The data have been phase folded using the best fit orbital period and epoch for WASP-85 A b, and binned using a bin width equivalent to 180s. We plot the original data in grey, and the best fit transit model in red. The lightcurves have been offset for clarity; for the same reason, we omit the error bars. The telescope, instrument, and date of observation are listed alongside each lightcurve. A slewing problem is responsible for the gaps in the lightcurve obtained by TRAPPIST on 2013-03-31.

of the IO:O observations, while for the Cousins R and RG filters we scale this ratio assuming perfect blackbody emission for the two stars. The third light contribution is added to the photometric transit model following the example of Southworth (2010). L_3 is strongly correlated with several other parameters, but we are able to model it in this fashion thanks to the measurement from IO:O.

We test for the presence of a long-term trend in RV using the additional jump parameter $d\gamma/dt$, the rate of

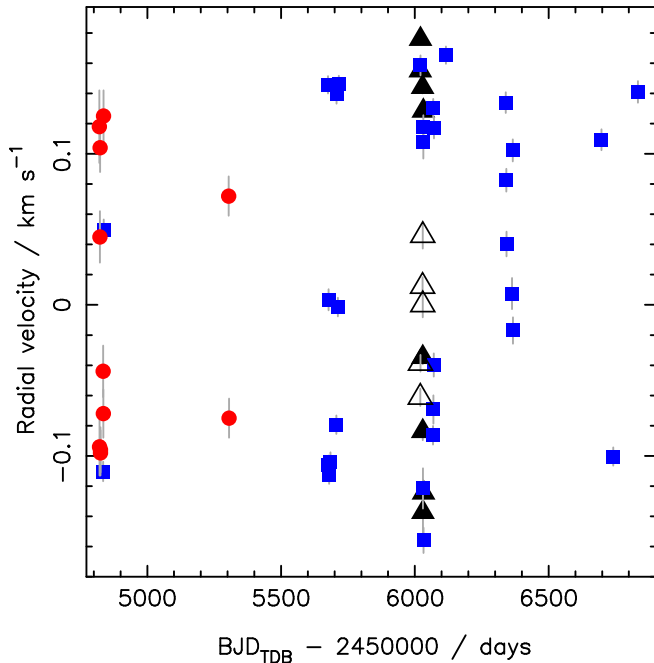


Figure 5. Radial velocity as a function of time. The best fit values of γ_i have been subtracted from each set of data. Despite the strong trend identified in our fit, we see no evidence for such trend over the full timespan of our observations. We conclude that the trend in γ_{HARPS} arises owing to the very short baseline of the HARPS observations.

change in systemic velocity with time. We find a significant improvement in the spectroscopic fit (parameterised using χ^2_{reduced}) when including such a trend, which we measure at $-110 \pm 3 \text{ m s}^{-1} \text{ yr}^{-1}$. However, we are sceptical that such a trend truly exists. The timespan of the HARPS observations is only twelve days, covering just over 4.5 orbits. This is insufficient to truly constrain any trend that might be present in the systemic velocity. Moreover, the CORALIE and SOPHIE data show no signs of any shift in γ over time. Even with the dilution caused by WASP-85 B, a trend of $-110 \pm 3 \text{ m s}^{-1} \text{ yr}^{-1}$ would be easily identifiable in Figure 5, as those data cover nearly 2000 days, over five years, and the postulated trend is on the order of the detected semi-amplitude. We therefore do not fit a trend in our final solution.

To test for an eccentric orbit, we use additional jump parameters of $\sqrt{e} \cos \omega$ and $\sqrt{e} \sin \omega$, where e is the orbital eccentricity and ω is the argument of periastron. We find eccentricities of between 0.0763 and 0.1774, depending on the inclusion or otherwise of a trend, and on whether the Bayesian penalty on stellar radius was applied. All are consistent with zero at $< 2\sigma$. We test the significance of these eccentricities using the F-test of Lucy & Sweeney (1971) to compare the fit to that of a circular orbit. We find that the probability of the eccentricity being detected by chance varies between 0.79 to 0.06, and therefore adopt a circular orbit in line with the advice in Anderson et al. (2012). Once again, the short timespan of the HARPS observations provides insufficient constraint even if the eccentricity was found to be significant.

One of the HARPS RV data has an uncertainty three times that of the other measurements, and a bisector span that is twice as large as the next greatest value. We carried out runs omitting this datum to check that it was not biasing our results. We found that removing this point made little difference to the significance of eccentricity, which we still find to favour a circular orbit but to be more significant in the absence of a long-term trend. Removing the datum led to only a small increase in the value of the fitted trend in γ . We note though that the eccentricity of the orbit tended to increase with the removal of the highly uncertain HARPS measurement. We attribute this to the spacing of the RV data in orbital phase, which leads to a fit dominated by the three data between phase 0 and phase 0.2.

The system parameters that we adopt are listed in Table 6, along with the prior values. In Figure 4 we display the phase-folded photometric lightcurves, overlaid with the best fit transit model. Note that the visible transit depth is shallower than the depth listed in Table 6 owing to the effect of the third light contribution. There is a notable difference in scatter between the two LT / IO:O lightcurves. This is likely to be a result of the comparison stars that were available for the data reduction process. For the lightcurve obtained on the night of 2013-01-12 there were two suitable comparison stars, which were fainter than WASP-85 by factors of 1.8 and 2.25. For the lightcurve obtained on the night of 2013-01-28, only one comparison star was available, and it was four times fainter than our target.

In Figure 6 we plot our RV data, overlaid with the best fit Keplerian orbit model for HARPS only analysis. We show all of our RV data to illustrate the effect of the dilution on the CORALIE and SOPHIE observations. The primary effect is a reduction in the semi-amplitude of the data (see also Table 6), though there is also increased scatter compared to the HARPS observations. We also show the residuals of the data compared to the plotted HARPS model. The sinusoidal structure present in the residuals for the CORALIE and SOPHIE data clearly indicates the reduced semi-amplitude.

This reduced semi-amplitude for the CORALIE and SOPHIE data is expected given the cross-correlation method by which we derive their RV measurements. WASP-85 B is relatively constant in RV, and thus the peak of the CCF will be constant in velocity space. The CCF for WASP-85 A, however, will move in velocity space. The close proximity of the two spares means that these CCFs merge to form a single, asymmetric CCF. The peak velocity will be biased towards the stationary position of WASP-85 B, effectively reducing the shift in velocity induced by the planet, and leading to a smaller semi-amplitude.

4. DISCUSSION

4.1. Diluted observations

We test the effect of the dilution on the parameters that we determine by carrying out several different analyses. We start by fitting the photometry and HARPS RVs using the same initial conditions, but without the additional third light term for the photometry. This run finds a transit depth of 0.0132 ± 0.0001 , some 50 percent smaller than the depth when accounting for the contam-

Table 6

System parameters for WASP-85 A and WASP-85 A b. We also list the Bayesian priors applied in the course of the MCMC analysis.

Parameter	Symbol	Value	Units
<i>Priors</i>			
Projected rotation velocity	$v \sin I_*$	3.41 ± 0.89	km s^{-1}
Effective temperature	T_{eff}	5685 ± 65	K
Metallicity	[Fe/H]	0.08 ± 0.10	dex
Flux ratio	L_3	0.50 ± 0.02	Cousins R filter
Flux ratio	L_3	0.50 ± 0.02	RG filter
Flux ratio	L_3	0.54 ± 0.02	Sloan z' filter
<i>Model parameters</i>			
Orbital period	P	2.6556734 ± 0.0000008	days
Epoch of mid-transit	t_0	6311.02659 ± 0.00010	BJD _{TDB}
Transit duration	T_{dur}	0.1118 ± 0.0003	days
Planet:star area ratio	R_p^2/R_*^2	0.0265 ± 0.0007	
Impact parameter	b	$0.044^{+0.037}_{-0.028}$	
RV semi-amplitude	K_{HARPS}	172.7 ± 4.8	m s^{-1}
	$K_{\text{CORALIE}}^\dagger$	132.8 ± 1.7	m s^{-1}
	$K_{\text{SOPHIE}}^\dagger$	$112.5^{+6.2}_{-6.5}$	m s^{-1}
Systemic velocity	γ_{HARPS}	13.5922 ± 0.0032	km s^{-1}
	$\gamma_{\text{CORALIE}}^\dagger$	13.5335 ± 0.0013	km s^{-1}
	$\gamma_{\text{SOPHIE}}^\dagger$	13.4610 ± 0.0045	km s^{-1}
Effective temperature	T_{eff}	5920^{+49}_{-58}	K
Metallicity	[Fe/H]	0.10 ± 0.10	dex
Flux ratio	$L_{3,\text{WASP}}$	0.50 ± 0.01	
	$L_{3,\text{JGT}}$	0.46 ± 0.03	
	$L_{3,\text{IO:O 1}}$	0.53 ± 0.01	
	$L_{3,\text{IO:O 2}}$	0.51 ± 0.02	
	$L_{3,\text{EULER}}$	0.53 ± 0.01	
	$L_{3,\text{TRAPPIST 1}}$	0.49 ± 0.02	
	$L_{3,\text{TRAPPIST 2}}$	0.50 ± 0.02	
	$L_{3,\text{TRAPPIST 3}}$	0.53 ± 0.01	
	$L_{3,\text{TRAPPIST 4}}$	0.58 ± 0.02	
<i>Derived parameters</i>			
Ingress / egress duration	$T_{12} = T_{34}$	0.0157 ± 0.0002	days
Orbital inclination	i_p	$89.72^{+0.18}_{-0.24}$	°
Orbital eccentricity	e	0 (adopted)	
Stellar mass	M_*	1.06 ± 0.05	M_\odot
Stellar radius	R_*	0.94 ± 0.01	R_\odot
Stellar surface gravity	$\log g_*$	4.519 ± 0.007	(cgs)
Stellar density	ρ_*	1.29 ± 0.01	ρ_\odot
Planet mass	M_p	1.22 ± 0.05	M_{Jup}
Planet radius	R_p	1.48 ± 0.03	R_{Jup}
Planet surface gravity	$\log g_p$	3.105 ± 0.016	(cgs)
Planet density	ρ_p	0.375 ± 0.018	ρ_{Jup}
Scaled semi-major axis	a/R_*	0.1138 ± 0.0003	
Semi-major axis	a	0.0382 ± 0.0006	AU
Planet equilibrium temperature	$T_{\text{P,A=0}}$	1412 ± 13	K

Notes: †: values of γ and K for the CORALIE and SOPHIE data were determined through a run using all three sets of RV data. This run did not significantly change the other model or derived parameters.

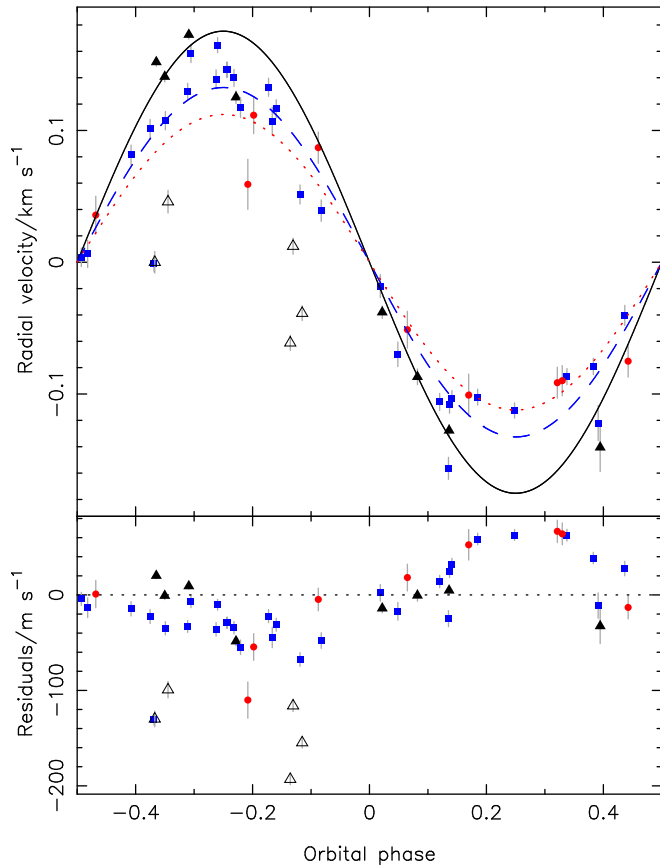


Figure 6. *Upper panel:* Radial velocity data for WASP-85, phase folded using the best fit orbital period and epoch for WASP-85 A b. HARPS data for WASP-85 A are denoted by solid, black triangles, data for WASP-85 B by open, black triangles. CORALIE data are denoted by solid, blue squares. SOPHIE data are denoted by solid, red circles. The best fit γ_i value for each set of data has been subtracted to allow comparison. Overplotted is our best fit orbital solution as derived from our MCMC analysis using the HARPS data only (solid black line). Also shown are the Keplerian solutions derived using K for the CORALIE data (dashed blue line) and SOPHIE data (dotted red line). The data for WASP-85 B show strong variation, but it is not correlated with the phase of the planet’s orbital solution. *Lower panel:* Radial velocity residuals as compared to the best fit model shown in the upper panel. The effect of the dilution in reducing the semi-amplitude is clearly visible.

ination. This is what we would expect given the flux ratio that we observe for the two stars. This smaller transit depth leads to a stellar density of $0.88 \pm 0.04 \rho_{\odot}$, 32 percent smaller than the value we report in Table 6, and a planet radius of $1.21 \pm 0.03 R_{\text{Jup}}$, 18 percent smaller than the value we report.

To characterise the effect of the third light dilution on the CORALIE and SOPHIE RV data, we carry out an additional fit using the same initial conditions, but including all of our RV data. We find that this makes little difference to the reported solution, but does provide additional useful information on the level of dilution. For this analysis, we use a number of K_i jump parameters equal to the number of datasets. K_{SOPHIE} is significantly smaller than K_{CORALIE} , which is in turn significantly smaller than K_{HARPS} . This is as expected given the different instrument specifications, and the different levels of dilution that are expected in the three

sets of data. In Figure 6 we plot all RV data to illustrate this point; note that the residuals are relative to the RV curve computed using K_{HARPS} .

As expected, the inclusion of the CORALIE and SOPHIE data reduces the magnitude of the trend in systemic velocity to zero.

We also test the effect of the diluted RVs on the planet mass that we derive by carrying out runs using the CORALIE data or SOPHIE data in place of the HARPS RVs. When using the CORALIE RVs we find a planet mass of $0.93 \pm 0.01 M_{\text{Jup}}$, 25 percent smaller than the value we find using the HARPS data. With the SOPHIE data, we find $M_{\text{p}} = 0.79 \pm 0.05 M_{\text{Jup}}$, 36 percent smaller than the HARPS result. These discrepancies match the differences that in K_i that we find when fitting all of the RV data simultaneously, as expected.

We estimate the RV signature that would be induced in WASP-85 A by the binary companion. We calculate an expected RV semi-amplitude of $K_{\text{binary}} = 1180 \text{ m s}^{-1}$ using the orbital period implied by the change in position angle. The greatest negative rate of change of RV occurs at phase 0; adopting this as our initial condition, we calculate $\Delta \text{RV} = -0.04 \text{ m s}^{-1}$ over the course of one year.

4.2. Binary companion

WASP-85 is listed as a known binary in the Washington Double Star catalogue (WDS). We obtained the full set of WDS measurements for the system, which stretch back to 1881. We also measured the position angle and angular separation of the companion star through careful analysis of EulerCAM observations taken on 2012 February 7th.

In Figure 7 we show both the binary angular separation and the binary position angle as a function of calendar date. The change in binary separation appears to be roughly periodic, with a period of approximately 30 years. However without error bars for the WDS data, it is likely that this is just random scatter. More high precision measurements of the separation will be needed to determine whether this variation is real; the upcoming GAIA mission will be of great help in this.

The position angle of the binary shows a clear, long-term, decreasing trend. This is a clear indication of orbital motion for the binary, and suggests an orbital period of $\gtrsim 3000$ years. This change of position angle suggests that the planet is misaligned from the plane of the binary. Using the distance listed in Table 3, the mean separation of $1.5''$ corresponds to a distance between the stars of 186 AU. Using the masses that we estimate for the two components from our spectral analysis, and assuming a circular orbit, this indicates a period of 1828 years, far less than the 3000 years suggested by the position angle change. The reverse transformation, from $P_{\text{binary}} = 3000$ years, gives a binary distance of 259 AU; again, this is discrepant with the separation derived value. This mismatch suggests that the binary orbit is inclined relative to our line of sight by $\approx 45^\circ$, again indicating a misalignment with the planet’s orbital plane.

The presence of the binary companion at < 259 AU from the planet host star suggests that the protoplanetary disc was likely truncated, limiting the quantity of material available for planet formation. Exploring this possibility is beyond the scope of this paper, but could be an interesting subject for future work.

Table 7

Position angles and angular separations for the binary star BD+07°2474 (WASP-85 AB). The majority of the measurements were obtained from the Washington Double Star catalogue. The most recent datum (marked with *) was obtained through analysis of images from EulerCAM, taken on 2012 February 7th.

Date (year)	Position Angle (degrees)	Angular Separation (arc sec)
1881.32	114.2	1.32
1888.351	113.1	1.66
1898.215	112.5	1.62
1898.40	111.2	1.58
1904.138	112.2	1.45
1909.14	115.4	1.29
1911.98	114.6	1.43
1914.32	114	1.34
1925.22	113.6	1.43
1925.31	110.7	1.68
1925.36	114.4	1.5
1928.31	111.1	1.52
1928.35	111.2	1.65
1944.11	112.2	1.3
1944.87	109	1.43
1954.11	106.3	1.62
1974.286	105.2	1.56
1975.16	104.3	1.32
1981.24	103.9	1.8
2010.287	99.9	1.24
2012.107*	99.62 ± 0.41	1.48 ± 0.01

4.3. Highly active stars

Comparing the Ca II H+K indices for the two stars to the sample of Jenkins et al. (2006, 2008, 2011), we find that both stars fall within the ‘very active stars’ region of Figure 4 in Jenkins et al. (2006). This is confirmed by Figure 10 of Jenkins et al. (2008) and Figure 6 of Jenkins et al. (2011), where in both cases the two stars fall within the secondary, ‘active’ peak in the $\log(R'_{\text{hk}})$ distribution. Comparison to the sample of Henry et al. (1996) shows that both stars fall in the ‘active’ class of stars.

Comparing to the sample of planet hosting stars examined by Knutson et al. (2010), we see that WASP-85 A is more active than all but one of the stars considered. Only CoRoT-2 is more active. It may be that we have simply observed the system at the peak of the activity cycle, leading to an apparently greater level of activity. However, if we consider the solar cycle then the typical variation is ≈ 0.2 dex; converting the solar Ca II H+K values presented in Livingston et al. (2007) indicates values of $\log(R'_{\text{hk}}) = -4.978$ and -4.803 at solar minimum and maximum, respectively. Measurements of activity during the Maunder Minimum (Donahue & Bookbinder 1998) indicate $\log(R'_{\text{hk}}) = -5.102$ during that particularly inactive period in the Sun’s life, giving a pessimistic variation from maximum of ~ 0.3 dex. If we apply this to WASP-85 A, then even at stellar ‘minimum’ it will be more active than the Sun at solar maximum, and will still be classified in the ‘active’ class of Henry et al. (1996). It therefore seems that these stars are unusually active for solar-type stars.

The amplitude of rotational variability in K-dwarfs can reach a few percent for periods ~ 15 days

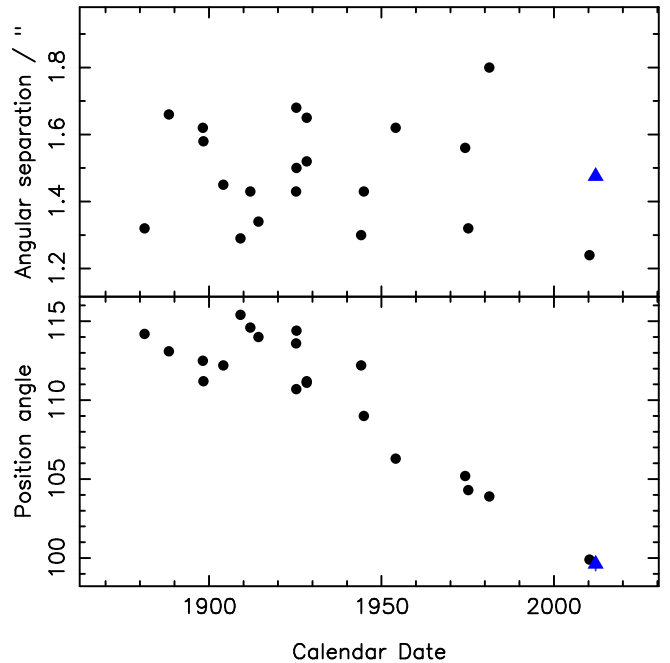


Figure 7. *Upper panel:* Angular separation of the two binary components as a function of calendar date. There appears to be short term variation with a period of approximately 30 years. The minimum separation implies an orbital distance of ~ 150 AU. *Lower panel:* Binary position angle as a function of calendar date. There is a clear, long-term trend for decreasing position angle. This suggests an orbital period for the binary of $\gtrsim 3000$ years. In both panels, black circles indicate data obtained from the Washington Double Star database, while blue triangles indicate data derived from EulerCam observations.

(Collier Cameron et al. 2009). It is therefore possible that the modulation observed in the WASP lightcurve originates from WASP-85 B. The negative correlation that we observe between the HARPS bisector span and RV measurements for WASP-85 B suggest that this might be the case. Though it is fainter, the difference in magnitude is such that the companion contributes significant light (as can be seen from the flux ratio of the two stars). Moreover the projected rotational velocities of the two stars are similar, and both are compatible with the measured rotation period. This degeneracy could be broken by careful, high resolution photometry of the two stars to check their individual rotation periods, or by measurement of the stellar inclinations. If either star is significantly inclined relative to the line of sight, then its true rotation period would be significantly shorter, and thus incompatible with the period determined from the WASP photometry.

4.4. K2 observations

During our campaign of follow-up observations of WASP-85 A b, a search of the proposed K2 fields revealed that the planetary system was visible in the Campaign 1 field. We proposed short cadence observations of WASP-85 under K2 proposal GO1041, and the system was selected for observation by K2. Four other K2 Campaign 1 proposals (GO1032, GO1054, GO1059, and GO1005) that included WASP-85 were also selected, three for long cadence observations and one for short cadence observations of the double star.

On the release of the Campaign 1 data, we downloaded the long cadence data for WASP-85 (short cadence data were not immediately available), extracted the photometric data, and corrected it for the systematic effect of pointing drift. This has been identified as the greatest source of error in the K2 lightcurves (Vanderburg & Johnson 2014). Our detrending method is similar to that developed by Vanderburg & Johnson, and has been previously described in Armstrong et al. (2014). Briefly, we use the centroid positions to create a 2D surface of raw flux as a function of the centroid’s position on the CCD. We then bin this data evenly by both row and column, and linearly interpolate the median flux from each bin to create a variability map. We divide the raw photometry by this surface map to create a corrected flux measurement that is decor related from the spacecraft’s pointing.

The upper panel of Figure 8 shows the detrended flux as a function of time. The planetary transits are clearly visible where they extend below the stellar lightcurve. Also apparent is the signature of stellar activity; the variations caused by the activity of one or both components of WASP-85 A B appears to be aperiodic at first glance, but this may result from star spot evolution. An initial Lomb-Scargle periodogram analysis of the lightcurve implies a period of 6.66 days for the variability, roughly commensurate with half of the rotation period determined from the WASP data.

The amplitude of the activity signal is approximately half the transit depth. The lower panel of Figure 8 shows the detrended K2 data phase folded on the best fit ephemeris from Table 6. We show only a small window around phase 0 to focus on the planetary transit, and have corrected for the stellar activity using a simple median filter with a window size of 1/100 times the length of the time series. This simple correction for activity leads to slightly increased scatter between contact points two and three of the transit.

The transit depth is approximately 0.016 magnitudes, less than the transit depth listed in Table 6. This is to be expected given the large pixel scale of the Kepler spacecraft’s CCD, which means that the stellar components of the system will be blended together as was the case for our other photometry. The depth discrepancy is as expected given the Kepler passband, the peak transmission of which roughly coincides with the peak transmission of the Johnson R filter (Rowe et al. 2009).

Analysis of the K2 data is ongoing, and incorporates both the long cadence data presented here and the short cadence data that was also collected by K2. The results of this analysis will be presented in a follow-up paper.

5. SUMMARY

We have presented the discovery of WASP-85 A b, a hot Jupiter planet orbiting the brighter component of BD+07°2474 every 2.66 days. The planet has a mass of $M_p = 1.09 \pm 0.03 M_{\text{Jup}}$ and a radius of $R_p = 1.44 \pm 0.02 R_{\text{Jup}}$. The host star is similar to the Sun, but has super-solar metallicity, while the companion is a cooler K-dwarf of similar magnitude. The Ca II H+K activity indices for the two stars indicate that both are strongly active, particularly when compared to other hot Jupiter hosts.

Our photometric observations of WASP-85 are con-

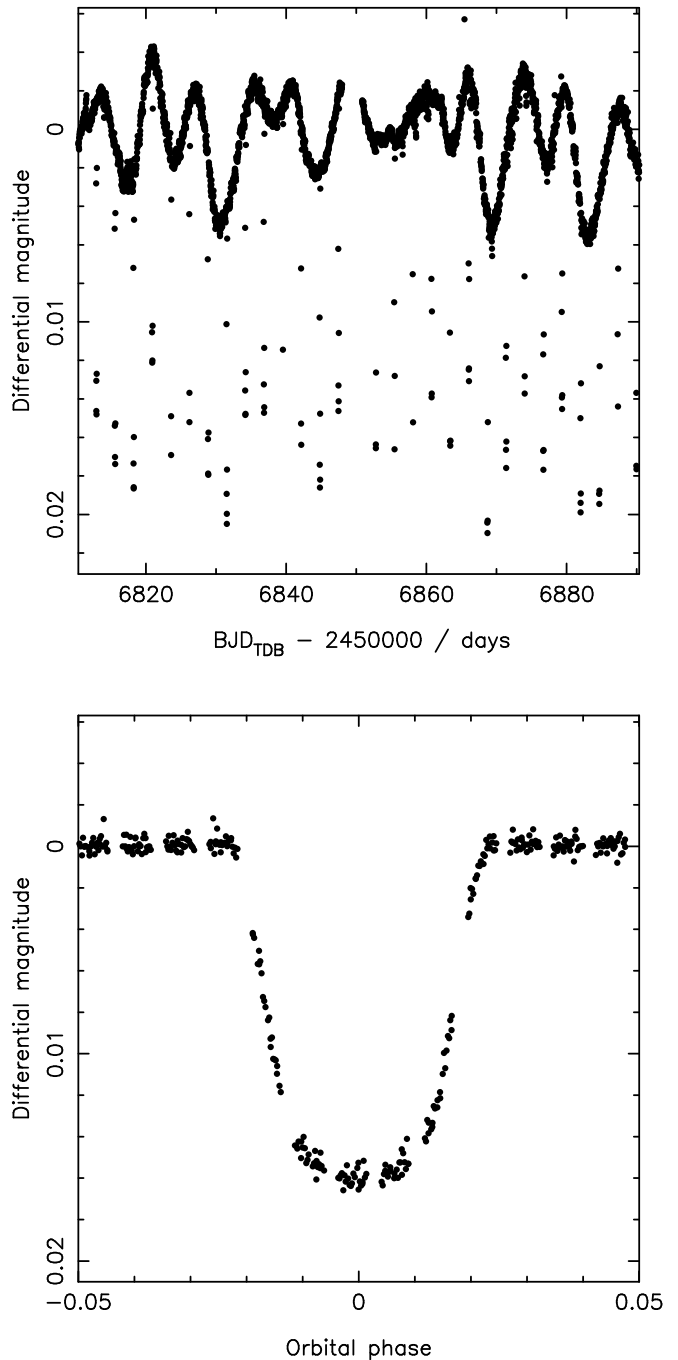


Figure 8. *Upper panel:* K2 long cadence photometry of BD+07°2474. The planetary transit signatures are clearly visible, as is variation arising from stellar activity. This stellar activity signal is of lower amplitude than the planetary transits. The system was also observed in short cadence mode as part of K2 Campaign 1, under our proposal GO1041; this data was not available at time of publication. *Lower panel:* The K2 long cadence lightcurve, phase folded on the best fit ephemeris from Table 6. We show a small window around phase 0 to focus on the planetary transit. Stellar activity has been corrected for using a simple median filter. Uncertainties are plotted in both panels, but are smaller than the size of the data points.

tain light from both binary components, necessitating the addition of a third light component to the standard transit model, and the modification of our standard WASP analysis routines. Spectroscopic observations with CORALIE and SOPHIE are also diluted by the companion, so we use only radial velocity data obtained with HARPS to perform our modelling. We find that the primary effect of the dilution is to decrease the radial velocity semi-amplitude for the affected datasets. If we fail to account for the contamination of the photometry, the derived planet radius decreases by 18 percent.

The binary position angle shows a clear, long-term, negative trend that suggests an orbit of $\gtrsim 3000$ years. This is at odds with the period derived from the mean binary angular separation, indicating that the binary is likely inclined relative to our line of sight by $\approx 45^\circ$. The planet's orbit is therefore misaligned with the binary plane.

BD+07°2474 has been observed at short cadence as part of K2 campaign 1. We have presented the K2 long cadence lightcurve for the system, which clearly shows the variability resulting from stellar activity, with the planetary transits superposed. K2 is unable to distinguish the binary components. Analysis of this new data is ongoing, and will be presented in a follow-up paper.

My thanks go to Dr. Simon Walker for helpful discussions during the analysis process.

The WASP Consortium consists of representatives from the Universities of Keele, Leicester, The Open University, Queens University Belfast and St Andrews, along with the Isaac Newton Group (La Palma) and the Instituto de Astrofísica de Canarias (Tenerife). WASP-South is hosted by the SAAO and SuperWASP-North by the Isaac Newton Group and the Instituto de Astrofísica de Canarias; we gratefully acknowledge their ongoing support and assistance. The SuperWASP and WASP-S cameras are operated with funds made available from Consortium Universities and the STFC. TRAPPIST is funded by the Belgian Fund for Scientific Research (Fond National de la Recherche Scientifique, FNRS) under the grant FRFC 2.5.594.09.F, with the participation of the Swiss National Science Foundation (SNF). The Liverpool Telescope is operated on the island of La Palma by Liverpool John Moores University in the Spanish Observatorio del Roque de los Muchachos of the Instituto de Astrofísica de Canarias with financial support from the UK Science and Technology Facilities Council. FC. M. G. and E. J. are FNRS Research Associates. L. D. is an FNRS/FRIA Doctoral Fellow. AHMJT is a Swiss National Science Foundation fellow under grant number P300P2-147773. This research has made use of NASA's Astrophysics Data System Bibliographic Services, the ArXiv preprint service hosted by Cornell University, the Washington Double Star Catalog maintained at the U.S. Naval Observatory, and the VizieR catalogue access tool, CDS, Strasbourg, France. The original description of the VizieR service was published in *A&AS* 143, 23.

Facilities: SuperWASP, Euler1.2, Liverpool:2m, ESO:3.6m, OHP:1.93m

REFERENCES

- Abt H. A., Levy S. G., 1976, *ApJS*, 30, 273
- Alonso R. et al., 2004, *ApJ*, 613, L153
- Anderson D. R. et al., 2012, *MNRAS*, 422, 1988
- Anderson D. R. et al., 2014, *MNRAS*, 445, 1114
- Armstrong D. J. et al., 2014, arXiv:1411.6830
- Asplund, M., Grevesse, N., Sauval, A.J., & Scott, P., 2009, *ARA&A*, 47, 481
- Baglin A. et al., 2006, in '36th COSPAR Scientific Assembly', 3749
- Bakos G. Á., Lázár J., Papp I., Sári P., Green E. M., 2002, *PASP*, 114, 974
- Barnes S. A., 2010, *ApJ*, 722, 222
- Barnes S. A., Kim Y.-C., 2010, *ApJ*, 721, 675
- Beatty T. G. et al., 2012, *ApJ*, 756, L39
- Borucki W. J. et al., 2010, *Science*, 327, 977
- Bouchy F. et al., 2009, *A&A*, 505, 853
- Bouchy F., Díaz R. F., Hébrard G., Arnold L., Boisse I., Delfosse X., Perruchot S., Santerne A., 2013, *A&A*, 549, A49
- Brown D. J. A. et al., 2012, *ApJ*, 760, 139
- Brown D. J. A., 2014, *MNRAS*, 442, 1844
- Buchhave L. A. et al., 2011, *ApJS*, 197, 3
- Charbonneau D., Brown T. M., Latham D. W., Mayor M., 2000, *ApJ*, 529, L45
- Claret A., 2000, *A&A*, 363, 1081
- Claret A., 2004, *A&A*, 428, 1001
- Collier Cameron A. et al., 2007, *MNRAS*, 380, 1230
- Collier Cameron A. et al., 2009, *MNRAS*, 400, 451
- Demarque P., Woo J.-H., Kim Y.-C., Yi S. K., 2004, *ApJS*, 155, 667
- 'Cool Stars, Stellar Systems and the Sun', 1998, *Astronomical Society of the Pacific Conference Series*, 154, eds. Donahue R. A., Bookbinder J. A.
- Dotter A., Chaboyer B., Jevremović D., Kostov V., Baron E., Ferguson J. W., 2008, *ApJS*, 178, 89
- Doyle, A.P., Smalley, B., Maxted, P.F.L., et al., 2013, *MNRAS*, 428, 3164
- Doyle, A.P., Davies, G.R., Smalley, B., Chaplin, W.J., Elsworth, Y., 2014, *MNRAS*, 444, 3592
- Duquennoy A., Mayor M., 1991, *A&A*, 248, 485
- Eastman J., Siverd R., Gaudi B. S., 2010, *PASP* 122, 935
- Gao S., Liu C., Zhang X., Justham S., Deng L., Yang M., 2014, *ApJ*, 788, L37
- Girardi L. et al., 2010, *ApJ*, 724, 1030
- Gray D.F., 2008, 'The observation and analysis of stellar photospheres', 3rd Edition (Cambridge University Press), p. 507.
- Henry T. J., Soderblom D. R., Donahue R. A., Baliunas S. L., 1996, *AJ*, 111, 439
- Howell S. B. et al., 2014, *PASP*, 126, 398
- Jehin E. et al., 2011, *The Messenger*, 145, 2
- Jenkins J. S. et al., 2006, *MNRAS*, 372, 163
- Jenkins J. S., Jones H. R. A., Pavlenko Y., Pinfield D. J., Barnes J. R., Lyubchik Y., 2008, *A&A*, 485, 571
- Jenkins J. S. et al., 2011, *A&A*, 531, A8
- Knutson H. A., Howard A. W., Isaacson H., 2010, *ApJ*, 720, 1569
- Lendl M. et al., 2012, *A&A*, 544, A72
- Livingston W., Wallace L., White O. R., Giampapa M. S., 2007, *ApJ*, 657, 1137
- Lucy L. B., Sweeney M. A., 1971, *AJ*, 76, 544
- Magain P., 1984, *A&A*, 134, 189
- Marigo P., Girardi L., Bressan A., Groenewegen M. A. T., Silva L., Granato G. L., 2008, *A&A*, 482, 883
- Mamajek E. E., Hillenbrand L. A., 2008, *ApJ*, 687, 1264
- Mandel K., Agol E., 2002, *ApJ*, 580, L171
- Maxted P. F. L. et al., 2011, *PASP*, 123, 547
- Maxted P. F. L. et al., 2013, *PASP*, 125, 48
- Maxted P. F. L., Serenelli A. M., Southworth J., 2014, arXiv:1412.7891
- McCullough P. R., Stys J. E., Valenti J. A., Fleming S. W., Janes K. A., Heasley J. N., 2005, *PASP*, 117, 783
- Neveu-VanMalle M. et al., 2014, arXiv:1409.7566
- Noyes R. W., Hartmann L. W., Baliunas S. L., Duncan D. K., Vaughan A. H., 1984, *ApJ*, 279, 763
- Pepper J. et al., 2007, *PASP*, 119, 923
- Perruchot S. et al., 2008, in in 'Society of Photo-Optical Instrumentation Engineers (SPIE) Conference Series', 7014
- Pollacco D. L. et al., 2006, *PASP*, 118, 1407
- Pollacco D. et al., 2008, *MNRAS*, 385, 1576

- Press W. H., Rybicki G. B., 1989, *ApJ*, 338, 277
- Queloz D., Mayor M., Naef D., Santos N., Udry S., Burnet M., Confino B., 2000, in Bergeron J., Renzini A., eds, *The VLT Opening Symposium: From Extrasolar Planets to Cosmology*, Springer-Verlag, Berlin, p. 548
- Queloz D. et al., 2001, *A&A*, 379, 279
- Raghavan D. et al., 2010, *ApJS*, 190, 1
- Roell T., Neuhäuser R., Seifahrt A., Mugrauer M., 2012, *A&A*, 542, A92
- Rowe J. F. et al., 2009, in 'Transiting Planets', *Proceedings of IAU Symposium 253*, eds. Pont F., Sasselov D., Holman M. J., p. 121
- Santerne A., Moutou C., Bouchy F., 2011, in 'The astrophysics of planetary systems: formation, structure, and dynamical evolution', *Proceedings of IAU Symposium 276*, eds. Sozzetti A., Lattanzi M. G., Boss A. P., p. 549
- Schwarz G. E., 1978, *Annals of Statistics*, 6, 461
- Serenelli A. M., Bergemann M., Ruchti G., Casagrande L., 2013, *MNRAS*, 429, 3645
- Sestito, P. & Randlich, S., 2005, *A&A*, 442, 615
- Southworth J., 2010, *MNRAS*, 408, 1689
- Southworth, J., 2011, *MNRAS*, 417, 2166
- Sozzetti A., Torres G., Charbonneau D., Latham D. W., Holman M. J., Winn J. N., Laird J. B., O'Donovan F. T., 2007, *ApJ*, 664, 1190
- Steele I. A. et al., 2004, in 'Society of Photo-Optical Instrumentation Engineers (SPIE) Conference Series', 5489
- Torres G., Andersen J. and Giménez A., 2010, *A&A Rev.*, 18, 67
- Vanderburg A., Johnson J. A., 2014, *PASP*, 126, 948
- Wang J., Fischer D. A., Xie J.-W., Ciardi D. R., 2014, *ApJ*, 791, 111
- Weiss A., Schlattl H., 2008, *Ap&SS*, 316, 99
- Wilson D. M. et al., 2008, *ApJ*, 675, L113
- Zechmeister M., Kürster M., 2009, *A&A*, 496, 577

